AGU PUBLICATIONS

Geophysical Research Letters

RESEARCH LETTER
10.1002/2015GL063701

Key Points:
- In the warm pool, downwelling motion has a leading role in subsurface warming
- There is a sharp transition at 170°E in the generation of the heat buildup
- Results are consistently reproduced by a set of ocean assimilation products

Supporting Information:
- Figures S1–S6

Correspondence to:
J. Ballester,
joanballester@caltech.edu

Citation:
Ballester, J., S. Bordoni, D. Petrova, and X. Rodó (2015), On the dynamical mechanisms explaining the western Pacific subsurface temperature buildup leading to ENSO events, *Geophys. Res. Lett.*, *42*, 2961–2967, doi:10.1002/2015GL063701.

Received 2 MAR 2015
Accepted 18 MAR 2015
Accepted article online 24 MAR 2015
Published online 19 APR 2015

On the dynamical mechanisms explaining the western Pacific subsurface temperature buildup leading to ENSO events

Joan Ballester[1,2], Simona Bordoni[1], Desislava Petrova[2], and Xavier Rodó[2,3]

[1]Environmental Science and Engineering, California Institute of Technology, Pasadena, California, USA, [2]Institut Català de Ciències del Clima, Barcelona, Spain, [3]Institució Catalana de Recerca i Estudis Avançats, Barcelona, Spain

Abstract Despite steady progress in the understanding of El Niño–Southern Oscillation (ENSO) in the past decades, questions remain on the exact mechanisms explaining the heat buildup leading to the onset of El Niño (EN) events. Here we use an ensemble of ocean and atmosphere assimilation products to identify mechanisms that are consistently identified by all the data sets and that contribute to the heat buildup in the western Pacific 18 to 24 months before the onset of EN events. Meridional and eastward heat advection due to equatorward subsurface mass convergence and transport along the equatorial undercurrent are found to contribute to the subsurface warming at 170°E–150°W. In the warm pool, instead, surface horizontal convergence and downwelling motion have a leading role in subsurface warming. The picture emerging from our results highlights a sharp dynamical transition at 170°E near the level of the thermocline.

1. Introduction

El Niño–Southern Oscillation (ENSO) is the most energetic climate signal after the seasonal cycle, the major source of interannual variability worldwide and a dominant driver of climate teleconnections [*Ballester et al.,* 2013]. Its prominent amplitude in the tropical Pacific is essentially explained by the positive Bjerknes feedback [*Bjerknes,* 1969; *Wyrtki,* 1975], which involves a strong coupling between the Walker circulation, the zonal gradient of sea surface temperature and the longitudinal tilt of the thermocline [*Ballester et al.,* 2011]. Two main theories have been invoked to bound the amplitude and reverse the sign of interannual anomalies: the delayed oscillator theory, which explains this reversal through differential propagation speed of wind-induced oceanic Kelvin and Rossby waves [*Battisti,* 1988; *Schopf and Suarez,* 1988; *Wang,* 2002; *Fedorov and Brown,* 2009]; and the recharge oscillator, which emphasizes the time delay between anomalies in longitudinally averaged thermocline depth and eastern Pacific sea surface temperature [*Jin*, 1997a, 1997b; *Meinen and McPhaden,* 2000].

The western Pacific is a key region for understanding the oscillatory nature of ENSO and the generation of EN and La Niña (LN) events. It is characterized by the warm pool, an upper ocean area of very warm and well-mixed waters (supporting information Figures S1b and S2b), surface horizontal current convergence and subsurface divergence (supporting information Figure S3b) and therefore downwelling motion. This region represents the main energy source for deep atmospheric convection and basin-wide teleconnections [*Picaut et al.,* 1996], and as such, it modulates both the climate of the planet and the physical properties and dynamical processes occurring locally. The equatorial Pacific is characterized by a sharp upper ocean zonal salinity front near the warm pool edge around 160°E–180°E (supporting information Figure S1b), which results from the convergence of zonally advected low- (high-) salinity water masses from the western (central) Pacific (supporting information Figure S3b) [*Bosc et al.,* 2009]. The longitudinal contrast in surface salinity is in turn explained by both the intense thermally driven atmospheric convection and rainfall to the west (supporting information Figure S4b) and the strong trade winds and evaporation to the east (supporting information Figure S5b).

The interannual zonal migration of the Pacific warm pool is well known to be associated with the displacement of the areas of deep atmospheric convection, active precipitation, strong trade winds, and enhanced evaporation [*Singh et al.,* 2011]. These relationships explain the intimate link between ENSO variability and the zonal thermohaline structure of the upper equatorial Pacific, with increased (decreased) zonal contrast of temperature and salinity during LN (EN) events, when the area of maximum precipitation is enhanced in the western Pacific (is shifted to the central Pacific) and the trade winds and westward surface currents are strengthened

(relaxed) in the central Pacific (supporting information Figures S1, S2, S4, and S5). These associations determine the intensity and vertical extension of surface horizontal current convergence and downwelling motion in the warm pool, as well as the zonal position and vertical tilt of local isopycnals through simultaneous changes in both the warm pool edge and the salinity front (supporting information Figures S1 and S3).

2. Methods

Outgoing longwave radiation, latent heat flux and wind stress data are derived from the NCEP/NCAR reanalysis reanalysis [*Kalnay et al.,* 1996] and precipitation is from the Global Precipitation Climatology Project version 2.2 (GPCP v2.2) Combined Precipitation Data Set [*Adler et al.,* 2003]. Ocean variables are obtained from five assimilation products: GECCO, ORAS4, NEMOVAR-COMBINE, SODA2.1.6, and SODA2.2.6 [*Köhl and Stammer,* 2008; *Balmaseda et al.,* 2008, 2010, 2013; *Carton and Giese,* 2008]. Vertical velocity is diagnosed by integrating horizontal divergence down from the surface, with surface values assumed to be equal to the time tendency of sea surface height.

A 13 term running average (1/24, 1/12, …, 1/12, …, 1/12, 1/24) is used to calculate the interannual component of detrended monthly variables. EN events are chosen according to the classification of the Climate Prediction Center for the common period 1961–2001 of the assimilation data sets: December 1963, 1965, 1968, 1972, 1976, 1982, 1986, 1990, and 1997 [*Climate Prediction Center,* 2013]. In those cases in which EN conditions are observed in the tropical Pacific for two consecutive boreal winters (i.e.,1968/1969, 1976/1977, 1986/1987, and 1990/1991), only the first year is considered for the calculation of the composite anomalies, given that our main objective here is the description of the onset of these events. The 1994 event was excluded from the analyses because it was the continuation of a previous warm event starting in 1990, with warm sea surface temperature anomalies persisting in the central and eastern tropical Pacific for almost 6 years [*Trenberth and Hoar,* 1996]. A similar criterion is used for the selection of LN years: December 1964, 1970, 1973, 1975, 1984, 1988, 1995, and 1998.

The temperature tendency equation is analyzed with regard to the contribution of the zonal (U_{adv}), meridional (V_{adv}), and vertical (W_{adv}) heat advection components. These terms are expressed as

$$U_{adv}{}' = -\overline{u}\frac{\partial\theta'}{\partial x} - u'\frac{\partial\overline{\theta}}{\partial x} - u'\frac{\partial\theta'}{\partial x} + \overline{u'\frac{\partial\theta'}{\partial x}}, \tag{1}$$

$$V_{adv}{}' = -\overline{v}\frac{\partial\theta'}{\partial y} - v'\frac{\partial\overline{\theta}}{\partial y} - v'\frac{\partial\theta'}{\partial y} + \overline{v'\frac{\partial\theta'}{\partial y}}, \quad \text{and} \tag{2}$$

$$W_{adv}{}' = -\overline{w}\frac{\partial\theta'}{\partial z} - w'\frac{\partial\overline{\theta}}{\partial z} - w'\frac{\partial\theta'}{\partial z} + \overline{w'\frac{\partial\theta'}{\partial z}}, \tag{3}$$

where the overbar and the prime denote the decomposition of potential temperature (θ) and the zonal (u), meridional (v), and vertical (w) current velocities into their climatology and the nonclimatological anomalies, respectively.

3. Results

Figure 1 shows the longitude-depth composite of equatorial potential temperature and its time tendency before EN events, averaged for the ensemble of assimilation products. Note that the stippling denotes areas where anomalies are consistent among all assimilation products. The initial accumulation of subsurface warm waters in the western Pacific (Figure 1a) and the subsequent eastward movement along the equatorial thermocline (Figures 1b–1d) characterize the onset of EN events [*Jin*, 1997a, 1997b]. This propagation links opposite phases of the tilting mode at lags −21 and +00 (Figures 1a and 1d) with a transition period of increased zonally integrated equatorial subsurface heat content at lag −09 [*Meinen and McPhaden,* 2000] (Figure 1c). After reaching the upper eastern equatorial Pacific, the released heat is rapidly amplified by the Bjerknes feedback, leading to the fast growth of an EN event [*Ramesh and Murtugudde,* 2013].

The present study describes the ocean-atmosphere mechanisms explaining this initial subsurface warming in the western equatorial Pacific, with special emphasis on the spatial characterization of the

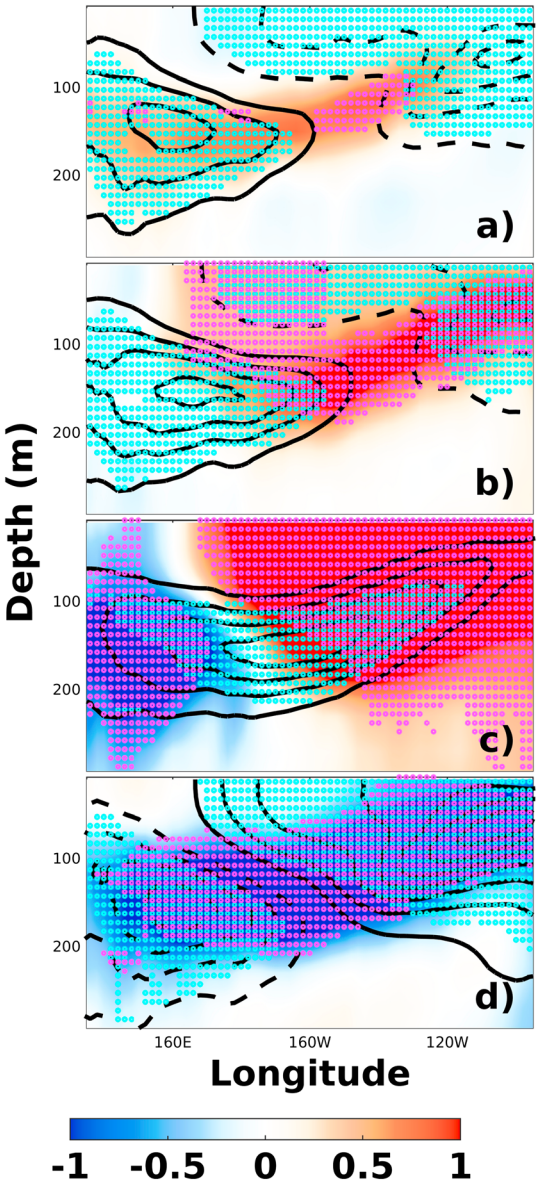

Figure 1. Evolution of equatorial temperature and its tendency during the onset of El Niño events. Multiproduct average of potential temperature (°C, contours) and its time tendency (°C/yr, shading) averaged over the equatorial band (2°S–2°N), and shown for lags 21 (a), 15 (b), 09 (c), 00, and (d) months before the major El Niño events. The temperature contour interval is 0.25°C, with solid (dashed) lines depicting positive (negative) anomalies. The purple (cyan) stippling denotes areas where shading (contour) anomalies have the same sign and magnitude larger than ±0.025°C/month (±0.25°C) for all members of the ensemble.

relative role that different processes play in this heat buildup. To this aim, Figure 2 shows the longitude-depth composites of ocean temperature, salinity, zonal velocity, and zonal, horizontal, and meridional divergence of ocean currents in the equatorial Pacific at 21 months before the mature phase of EN, while Figure 3 depicts the contribution of zonal, meridional, and vertical heat advection to the temperature tendency leading to the anomalies occurring at this lag.

On average, the peak of interannual LN-like conditions is found in the upper equatorial ocean at lag −21, with colder-than-normal waters in the central and eastern Pacific (contours in Figure 2). The subsequent shift of convection and precipitation to the far western Pacific increases the surface salinity in the easternmost edge of the climatological warm pool near 160°E–180°E (shading in Figure 2a), sharpening the zonal differences in surface salinity near the warm pool edge and the salinity front. Changes in both temperature and salinity increase the zonal contrast in upper ocean density and the local tilt of the isopycnals. At the same time, the enhanced trade winds in the central Pacific strengthen the westward south equatorial current near the warm pool edge and the salinity front (Figure 2b). This results in anomalous surface zonal (0–60 m) and horizontal (0–75 m) convergence in the western equatorial Pacific (shading in Figures 2c and 2d). The surface buoyancy loss, additional isopycnal tilting and enhanced surface westward circulation and horizontal current convergence result into the intensification of the downwelling motion, which contributes to the growth of the subsurface warm buildup.

The strengthening of the trades during LN-like conditions is also associated with the enhancement of the clockwise (counterclockwise) wind stress curl in the central off-equatorial north (south) Pacific, which together with the rise in dynamic height due to the accumulation of warm waters in the western Pacific, drives anomalous geostrophic Sverdrup transport toward the equator (shading in Figure 2e) [*Wyrtki,* 1981]. This subsurface-intensified meridional convergence is particularly strong in the western and central Pacific, where the strongest interannual ENSO-like zonal wind stress anomalies are found (cf. with supporting

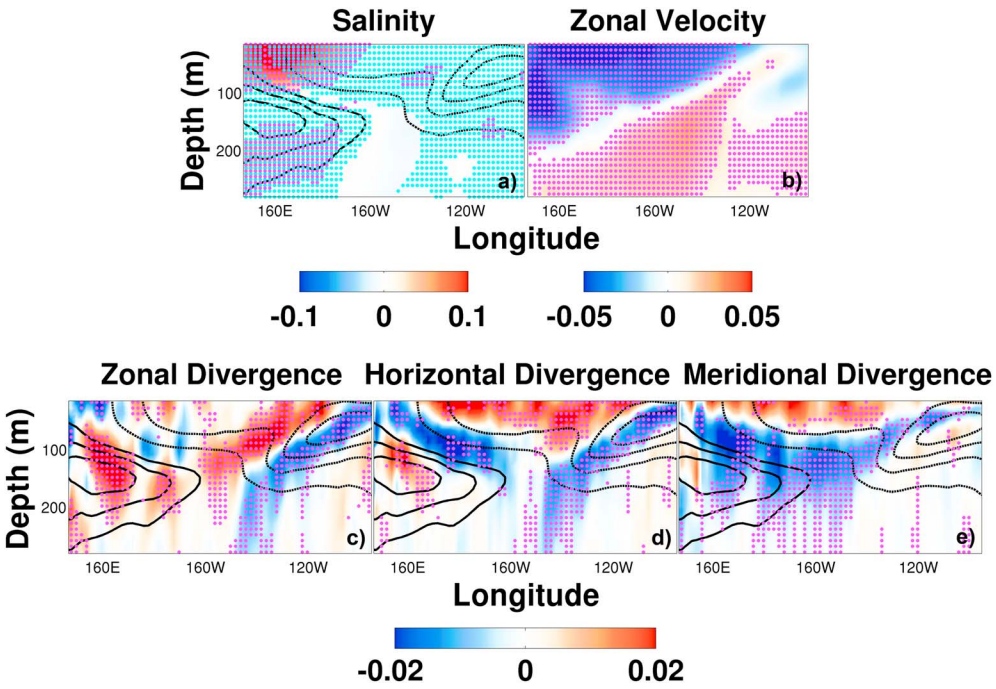

Figure 2. Multiproduct average of equatorial variables during the heat buildup leading to El Niño events. Potential temperature (°C, contours), (a) salinity (g/kg), (b) zonal velocity (m/s), and (c) zonal, (d) horizontal, and (e) meridional current divergence (10^{-6} 1/s). Composite anomalies are averaged over the equatorial band (2°S–2°N), and shown for lag 21 months before the major El Niño events. The temperature contour interval is 0.25°C, with solid (dashed) lines depicting positive (negative) anomalies. The purple (cyan) stippling denotes areas where shading (contour) anomalies have the same sign for all the members of the ensemble.

information Figure 5d). It is important to note that the meridional Sverdrup subsurface convergence is already present in the western and central Pacific at lag −30, when incipient LN-like conditions start to reinforce the trade winds (not shown). In the upper Ekman layer, the stronger-than-normal easterly wind stress generates anomalous meridional Ekman divergence (shading in Figure 2e). This configuration with surface meridional divergence and subsurface convergence results into an area of anomalous upper ocean upwelling motion to the east of the dateline (shading in Figure 2d). In the warm pool, anomalous zonal currents are strongly convergent in the surface and divergent in the subsurface (shading in Figure 2c). These zonal signals are locally stronger than the expected meridional Ekman-induced surface divergence and the meridional Sverdrup subsurface convergence, therefore inducing anomalous local downward motion to the west of 170°E (shading in Figure 2d).

The mechanisms described in Figure 2 are consistently observed in all the assimilation products considered in this study (supporting information Figure S6). Interestingly, the magnitude of surface temperature, salinity, and current anomalies and the associated subsurface warming vary coherently between products, so that the stronger these anomalies, the warmer the subsurface buildup. For example, the interproduct correlation between surface salinity (156°–166°E, 0–50 m) and subsurface potential temperature (156°–166°E, 100–130 m) is 0.98 ($p < 0.001$), with a regression coefficient of 3.91°C per g/kg. The only exception is GECCO, which underestimates the zonal surface convergence (subsurface divergence) in the warm pool compared to other products, and does not produce the patterns of meridional surface Ekman divergence (subsurface Sverdrup convergence) in the western and central equatorial Pacific observed in the other assimilation data sets. Interestingly, this is the assimilation product with the weakest subsurface heat buildup. The fact that GECCO is nevertheless able to reproduce the vertical structure of horizontal divergence in the warm pool, and therefore, the associated downwelling motion suggests that the contribution by the subsurface meridional mass convergence and subsurface eastward advection might be underestimated. The associated spread in the simulation of meridional divergence across the different assimilation products allows a rough estimate of the relative dependency between these variables in the western equatorial Pacific. Thus, the interproduct correlation between meridional upper ocean divergence (156°–166°E, 0–200 m) and subsurface potential

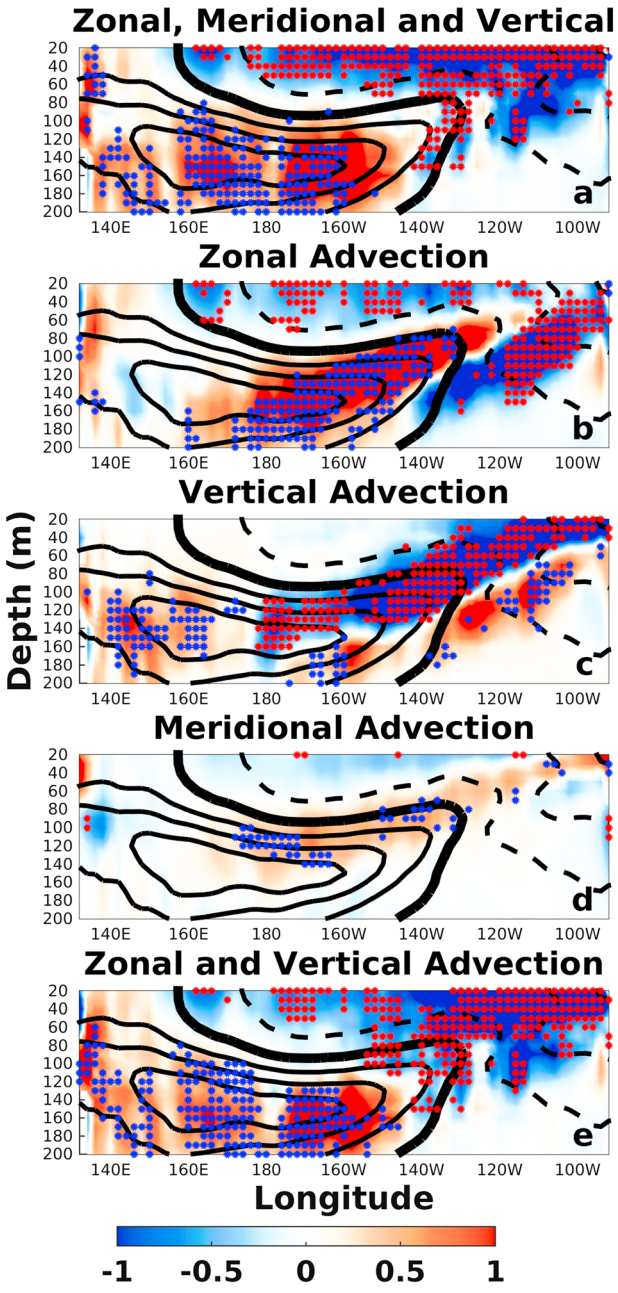

Figure 3. Multiproduct average of heat advection preceding the heat buildup leading to El Niño events. Tendency in potential temperature (°C/yr, contours) and zonal (Figures 3a, 3b, and 3e), meridional (Figures 3a and 3d), and vertical (Figures 3a, 3c, and 3e) heat advection (°C/yr). Composite anomalies are averaged over the equatorial band (2°S–2°N), and shown for lag 30 months before the major El Niño events. Note that this lag shows the temperature tendency that determines the anomalies that are later observed at lag −21. The contour interval is 0.25°C/yr, with solid (dashed) lines depicting positive (negative) anomalies. The stippling denotes areas where shading anomalies have the same sign for all the members of the ensemble.

temperature (156°–166°E, 100–130 m) is −0.90 ($p < 0.001$), with a regression coefficient of $-3.36 \cdot 10^7$°C per 1/s. Instead, surface horizontal convergence (156°–166° E, 20–60 m) is consistently observed in all the assimilation products, with a mean relationship of $-4.38 \cdot 10^7$°C per 1/s with subsurface potential temperature.

The analysis of the temperature tendency equation reveals that the sum of the zonal and vertical advection terms explains a large fraction of the spatial structure of the tendency in surface and subsurface heat anomalies in the equatorial Pacific (cf. shading and contours in Figures 3a and 3e). Vertical advection alone determines the subsurface warming to the west of 170° E (Figure 3c). Instead, to the east of the sharp transition at 170°E, the largest contribution comes from the combination of the zonal (Figure 3b) and vertical (Figure 3c) advection components (Figure 3e), as a result of the strengthening of the equatorial undercurrent and the advection of incipient subsurface temperature anomalies from the western to the central Pacific. Nevertheless, the meridional advection of heat is already contributing to the warming at the level of the thermocline to the east of 170°E (Figure 3d), even if at this early stage of the ENSO oscillation the thermocline has a tendency toward shallower depths in the eastern Pacific (contours in Figure 3). Note that to the west of 170°E, where the subsurface equatorward convergence of mass is as strong as in the central Pacific, the meridional advection of heat is weak because the meridional temperature gradient at the equator is small (not shown).

4. Summary and Discussion

The present work shows that the enhancement of the trade winds in the central equatorial Pacific increases the intensity of the westward circulation of the south equatorial current [*Yu and McPhaden,* 1999], strengthening the surface zonal and thus horizontal current convergence and downwelling motion near the anomalously tilted warm pool edge and salinity front. Additionally, we show that the vertical advection of heat plays a key role in the redistribution of water masses in the warm pool. Zonal and vertical currents are indeed intimately connected through the energy balance, because a significant

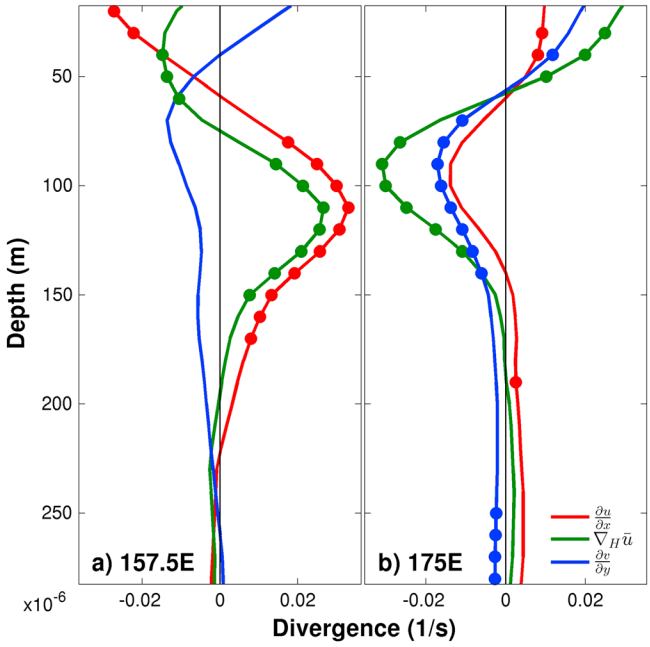

Figure 4. Vertical profiles of equatorial current divergence during the heat buildup leading to El Niño events. Multiproduct average of zonal (red), horizontal (green), and meridional (red) current divergence (1/s) at longitudes (a) 157.5°E and (b) 175°E, averaged over the equatorial band (2°S–2°N), and shown for lag 21 months before the major El Niño events. Dots denote depths where anomalies have the same sign for all the members of the multiproduct ensemble.

fraction of the wind power (whose interannual signal is dominated by the zonal component) is converted into buoyancy power [*Brown and Fedorov,* 2010]. This transfer explains how the energy supplied by enhanced trade winds to the westward south equatorial current in the central Pacific is converted into vertical mass fluxes in the western Pacific that distort local ocean isopycnals and deepen the thermocline [*Brown et al.,* 2011].

In this regard, results presented here provide a comprehensive description of the interaction between wind stress forcing in the central Pacific, oceanic circulation in the warm pool, and subsurface temperature and thermocline depth in the western equatorial Pacific starting about 2 years before the peak of EN. Figure 4 summarizes the relevant anomalies in horizontal current divergence for two representative equatorial locations to the west of the dateline. Near the warm pool edge and salinity front (i.e., 157.5°E, Figure 4a), we find downwelling motion from an upper layer (0–75 m) with horizontal convergence to a subsurface layer (75–190 m) with horizontal divergence. The decomposition of horizontal divergence into its zonal and meridional components reveals how at these long lead times different mechanisms contribute in an intricate way to the subsurface heat buildup. On the one hand, horizontal convergence near the surface (0–75 m) is to a large extent explained by surface (0–60 m) zonal convergence and to a lower extent by subsurface (40–75 m) meridional convergence. On the other hand, the subsurface layer (75–190 m) of horizontal divergence is almost entirely explained by the zonal component, characterized by the strengthening of the equatorial undercurrent in the central Pacific. Near the dateline (i.e., 175°E, Figure 4b), vertical profiles of horizontal divergence reveal a different regime, dominated by surface (0–60 m) zonal and meridional divergence and subsurface (60–190 m) zonal and meridional convergence.

These results are based on an ensemble of ocean assimilation products and to the extent these products can be regarded as faithfully capturing the observed dynamics, the anomalies that are consistently simulated by all the data sets can be used to validate previous modeling studies. For instance, *Yu and Mechoso* [2001] used a coupled ocean-atmosphere general circulation model to show that vertical advection contributes to the subsurface (80–145 m) cooling during the mature phase of El Niño (see their Figure 18c). For the sake of this discussion, we will here assume opposite anomalies for LN conditions, which would correspond to our results in Figure 3c. Despite the similarities with our results, the subsurface cooling due to vertical advection in *Yu and Mechoso* [2001] occurs in a broad longitudinal band extending from the western boundary to 150°W, while in the analysis products the subsurface warming due to vertical advection is confined to a very narrow range to the west of 170°E. Coherently, the distribution of horizontal divergence inferred from the assimilation products also shows a sharp transition at 170°E from surface (subsurface) horizontal convergence (divergence) to the west and divergence (convergence) to the east. The spatial characterization emerging from this work might prove useful in determining the relative role of the different processes involved in the generation of the heat buildup in the western Pacific, and ultimately in improving the predictability of ENSO at long lead times beyond the spring barrier.

Acknowledgments
J.B. gratefully acknowledges funding from the European Commission through a Marie Curie International Outgoing Fellowship of the 7th Framework Programme for Research (project MEMENTO from the FP7-PEOPLE-2011-IOF call). X.R. acknowledges funding from the EUFP7 project EUPORIAS. NCEP/NCAR and GPCP data are obtained from http://www.esrl.noaa.gov, and ocean variables are from http://icdc.zmaw.de.

The Editor thanks two anonymous reviewers for their assistance in evaluating this paper.

References

Adler, R. F., et al. (2003), The version-2 Global Precipitation Climatology Project (GPCP) monthly precipitation analysis (1979-present), *J. Hydrometeorol.*, *4*, 1147–1167, doi:10.1175/1525-7541(2003)004<1147:TVGPCP>2.0.CO;2.

Ballester, J., M. A. Rodríguez-Arias, and X. Rodó (2011), A new extratropical tracer describing the role of the western Pacific in the onset of El Niño: Implications for ENSO understanding and forecasting, *J. Clim.*, *24*, 1425–1437, doi:10.1175/2010JCLI3619.1.

Ballester, J., J. C. Burns, D. Cayan, Y. Nakamura, R. Uehara, and X. Rodó (2013), Kawasaki disease and ENSO-driven wind circulation, *Geophys. Res. Lett.*, *40*, 2284–2289, doi:10.1002/grl.50388.

Balmaseda, M. A., A. Vidard, and D. L. T. Anderson (2008), The ECMWF ocean analysis system: ORA-S3, *Mon. Weather Rev.*, *136*, 3018–3034, doi:10.1175/2008MWR2433.1.

Balmaseda, M. A., K. Mogensen, F. Molteni, and A. T. Weaver (2010), The NEMOVAR-COMBINE ocean re-analysis, *COMBINE Tech. Rep. No. 1*.

Balmaseda, M. A., K. Mogensen, and A. T. Weaver (2013), Evaluation of the ECMWF ocean reanalysis system ORAS4, *Q. J. R. Meteorol. Soc.*, *139*, 1132–1161, doi:10.1002/qj.2063.

Battisti, D. S. (1988), Dynamics and thermodynamics of a warming event in a coupled tropical atmosphere–ocean model, *J. Atmos. Sci.*, *45*, 2889–2919, doi:10.1175/1520-0469(1988)045<2889:DATOAW>2.0.CO;2.

Bjerknes, J. (1969), Atmospheric teleconnections from the equatorial Pacific, *Mon. Weather Rev.*, *97*, 163–172, doi:10.1175/1520-0493(1969)097<0163:ATFTEP>2.3.CO;2.

Bosc, C., T. Delcroix, and C. Maes (2009), Barrier layer variability in the western Pacific warm pool from 2000 to 2007, *J. Geophys. Res.*, *114*, C06023, doi:10.1029/2008JC005187.

Brown, J. N., and A. V. Fedorov (2010), How much energy is transferred from the winds to the thermocline on ENSO time scales?, *J. Clim.*, *23*, 1563–1580, doi:10.1175/2009JCLI2914.1.

Brown, J. N., A. V. Fedorov, and E. Guilyardi (2011), How well do coupled models replicate ocean energetics relevant to ENSO?, *Clim. Dyn.*, *36*, 2147–2158, doi:10.1007/s00382-010-0926-8.

Carton, J. A., and B. S. Giese (2008), A reanalysis of ocean climate using Simple Ocean Data Assimilation (SODA), *Mon. Weather Rev.*, *136*, 2999–3017, doi:10.1175/2007MWR1978.1.

Climate Prediction Center (2013), Cold and warm episodes by season. [Available at http://www.cpc.ncep.noaa.gov/products/analysis_monitoring/ensostuff/ensoyears.shtml Last accessed in January 2014.]

Fedorov, A. V., and J. Brown (2009), Equatorial waves, in *Encyclopedia of Ocean Sciences*, 2nd ed., edited by J. Steele, pp. 3679–3695, Academic Press. San Diego, Calif.

Jin, F. F. (1997a), An equatorial ocean recharge paradigm for ENSO. Part I: Conceptual model, *J. Atmos. Sci.*, *54*, 811–829, doi:10.1175/1520-0469(1997)054<0811:AEORPF>2.0.CO;2.

Jin, F. F. (1997b), An equatorial ocean recharge paradigm for ENSO. Part II: A stripped-down coupled model, *J. Atmos. Sci.*, *54*, 830–847, doi:10.1175/1520-0469(1997)054<0830:AEORPF>2.0.CO;2.

Kalnay, E., et al. (1996), The NCEP/NCAR 40-year reanalysis project, *Bull. Am. Meteorol. Soc.*, *77*, 437, doi:10.1175/1520-0477(1996)077<0437:TNYRP>2.0.CO;2.

Köhl, A., and D. Stammer (2008), Variability of the meridional overturning in the North Atlantic from the 50-year GECCO state estimation, *J. Phys. Oceanogr.*, *38*, 1913–1930, doi:10.1175/2008JPO3775.1.

Meinen, C. S., and M. J. McPhaden (2000), Observations of warm water volume changes in the equatorial pacific and their relationship to El Niño and La Niña, *J. Clim.*, *13*, 3551–3559, doi:10.1175/1520-0442(2000)013<3551:OOWWVC>2.0.CO;2.

Picaut, J., M. Ioualalen, C. Menkes, T. Delcroix, and M. J. McPhaden (1996), Mechanism of the zonal displacements of the Pacific warm pool: Implications for ENSO, *Science*, *274*, 1486–1489, doi:10.1126/science.274.5292.1486.

Ramesh, N., and R. Murtugudde (2013), All flavours of El Niño have similar early subsurface origins, *Nat. Clim. Change*, *3*, 42–46, doi:10.1038/nclimate1600.

Schopf, P. S., and M. J. Suarez (1988), Vacillations in a coupled ocean–atmosphere model, *J. Atmos. Sci.*, *45*, 549–566, doi:10.1175/1520-0469(1988)045<0549:VIACOM>2.0.CO;2.

Singh, A., T. Delcroix, and S. Cravatte (2011), Contrasting the flavors of El Niño-Southern Oscillation using sea surface salinity observations, *J. Geophys. Res.*, *116*, C06016, doi:10.1029/2010JC006862.

Trenberth, K. E., and T. J. Hoar (1996), The 1990–1995 El Niño-Southern Oscillation event: Longest on record, *Geophys. Res. Lett.*, *23*, 57–60, doi:10.1029/95GL03602.

Wang, B. (2002), Kelvin waves, in *Encyclopedia of Atmospheric Sciences*, edited by M. Shankar, pp. 1062–1068, Elsevier, Amsterdam.

Wyrtki, K. (1975), El Niño—The dynamic response of the equatorial Pacific Ocean to atmospheric forcing, *J. Phys. Oceanogr.*, *5*, 572–584, doi:10.1175/1520-0485(1975)005<0572:ENTDRO>2.0.CO;2.

Wyrtki, K. (1981), An estimate of equatorial upwelling in the Pacific, *J. Phys. Oceanogr.*, *11*, 1205–1214, doi:10.1175/1520-0485(1981)011<1205:AEOEUI>2.0.CO;2.

Yu, J. Y., and C. R. Mechoso (2001), A coupled atmosphere–ocean GCM study of the ENSO cycle, *J. Clim.*, *14*, 2329–2350, doi:10.1175/1520-0442(2001)014<2329:ACAOGS>2.0.CO;2.

Yu, X., and M. J. McPhaden (1999), Seasonal variability in the equatorial Pacific, *J. Phys. Oceanogr.*, *29*, 925–947, doi:10.1175/1520-0485(1999)029<0925:SVITEP>2.0.CO;2.